Available online at www.sciencedirect.com
SCIENCE DIRECT®
Journal of Fluorine Chemistry 125 (2004) 1715–1722
JOURNAL OF FLUORINE CHEMISTRY
www.elsevier.com/locate/fluor

Preparation of boron-doped semiconducting diamond films using BF_3 and the electrochemical behavior of the semiconducting diamond electrodes

Fujio Okino[a,*], Yukio Kawaguchi[a], Hidekazu Touhara[a], Kunitake Momota[b], Mikka Nishitani-Gamo[c], Toshihiro Ando[d], Atsushi Sasaki[e], Mamoru Yoshimoto[e], Osamu Odawara[f]

[a]*Faculty of Textile Science and Technology, Shinshu University, 3-15-1 Tokida, Ueda 386-8567, Japan*
[b]*Department of Research and Development, Morita Chemical Industries Company Limited, Higashimikuni 3-12-10, Yodogawa-ku, Osaka 532-0002, Japan*
[c]*Department of Applied Chemistry, Faculty of Engineering, Toyo University, 2100 Kujirai, Kawagoe 350-8585, Japan*
[d]*National Institute for Materials Science, 1-1 Namiki, Tsukuba 305-0044, Japan*
[e]*Materials and Structures Laboratory, Tokyo Institute of Technology, 4259 Nagatsuta, Midori, Yokohama 226-8503, Japan*
[f]*Department of Innovative and Engineered Materials, Interdisciplinary Graduate School of Science and Engineering, Tokyo Institute of Technology, 4259 Nagatsuta, Midori, Yokohama 226-8502, Japan*

Available online 14 October 2004

Abstract

Boron-doped semiconducting diamond films were prepared using BF_3 by microwave plasma assisted chemical vapor deposition. B-doping was confirmed by SIMS and Raman spectroscopic measurements and the B-doping levels were estimated. Electrochemical behaviors of boron-doped diamond thin-film electrodes prepared using B_2H_6 and BF_3 were studied by measuring cyclic voltammograms for anodic oxidation of 1,4-difluorobenzene in the liquid electrolyte, neat $Et_4NF{\cdot}4HF$. The results of the direct thermal interaction of elemental fluorine with hydrogenated and oxidized diamond surfaces are also presented.

Keywords: Diamond; Fluorination; BF_3; Boron-doping; SIMS; Cyclic voltammetry; Raman spectroscopy

1. Introduction

For the synthesis of boron-doped diamond (BDD) thin films by chemical vapor deposition (CVD), various boron-containing compounds, e.g., diborane [1–4], trimethylboron [5,6], trimethyl borate [7], tripropyl borate [8], h-BN [9], B_2O_3 [10–13] are used. Addition of boron not only makes synthesized diamond semiconducting but also affects various factors, e.g., growth rate, crystallinity and morphology of the diamond particles. Raman spectroscopy can provide useful information on the crystal quality. Interesting results have been reported on the Raman spectral changes of BDD [14]. Some halocarbons and halogens have been observed to enhance low temperature growth, nucleation density and crystal quality in the CVD synthesis of diamond thin films, thus economizing and improving the process [15–17]. As a typical monovalent element along with hydrogen, fluorine is expected to efficiently play the role of hydrogen, an indispensable component of the feed gas in the CVD diamond synthesis. Since BF_3 contains both boron and fluorine, it can be regarded not only as a boron source but also as a fluorine source that could affect the formation of diamond significantly.

Diamond has many distinguished properties, such as hardness, optical transparency, high thermal conductivity, corrosion resistance and chemical inertness. It is stable under harsh fluorination conditions; only the outermost

* Corresponding author. Tel.: +81 268 21 5393; fax: +81 268 21 5391.
E-mail address: fuokino@giptc.shinshu-u.ac.jp (F. Okino).

0022-1139/$ – see front matter © 2004 Elsevier B.V. All rights reserved.
doi:10.1016/j.jfluchem.2004.09.009

surface of the diamond is fluorinated by 1 atm elemental fluorine at 500 °C [18]. Under the same conditions graphite readily yields graphite fluoride $(CF)_n$ [19]. In the electrolytic preparation of fluorine at a graphite anode, this insulating $(CF)_n$ is eventually formed leading to the anode effect. This chemical inertness of diamond and its wide potential window [20–24] indicate that diamond can be used as an anode material for electrolytic production of fluorine and electrochemical fluorination.

In the present work BDD thin films were prepared using BF_3 by microwave plasma assisted CVD, and B concentration depth profiles were measured by secondary ion mass spectroscopy (SIMS) to confirm the doping of diamond with B using BF_3. Raman spectra were also taken to correlate the spectrum change with B-doping level. To our knowledge this is the first time that BF_3 was used as a boron source for BDD.

This paper presents the results of (1) fluorination of hydrogenated and oxidized diamond surfaces studied by diffuse reflectance infrared Fourier-transform (DRIFT) spectroscopy [18], (2) preparation of BDD thin films using BF_3, and (3) electrochemical behaviors of BDD thin-film electrodes made using B_2H_6 [25] and BF_3 [26] by measuring cyclic voltammograms (CV) for anodic oxidation of 1,4-difluorobenzene in the liquid electrolyte, neat $Et_4NF{\cdot}4HF$.

2. Results and discussion

2.1. Diffuse reflectance infrared Fourier-transform study of the direct thermal fluorination of diamond powder surfaces

Fig. 1 shows the DRIFT results of the fluorination of the hydrogenated diamond powder surface [18]. The spectrum before fluorination, spectrum (a), contains several peaks in the region 2800–2970 cm^{-1}. These are ascribed to C–H stretching vibrations of sp^3 hybridized bonding. In the spectrum after fluorination at −10 °C, spectrum (b), no C–H stretching vibrations were observed and, at the same time, new peaks appeared in the region 1000–1400 cm^{-1} with two maxima at 1085 and 1277 cm^{-1}. These are due to C–F stretching vibrations. This result indicates that substitution for hydrogen by fluorine molecules occurred even at −10 °C and resulted in fluorine being chemisorbed onto the diamond surface. With increasing reaction temperature, the C–F stretching vibrations increase in intensity. Four clear peaks at 1096, 1251, 1333, and 1347 cm^{-1} were observed in spectrum (g) after fluorination at 100 °C. The peak at 1347 cm^{-1} grew and slightly shifted to 1360 cm^{-1} with increasing the fluorination temperature. The peak at 1360 cm^{-1} can be assigned to either CF_2 or CF_3 group vibrations. The increase in intensity of the peak at 1360 cm^{-1} with reaction temperature suggests that the population density of fluorine increases to give CF_2 and CF_3 species. The peak at 1333 cm^{-1} is due to the C–C stretching vibrations of the diamond crystal lattice with the same frequency of the diamond Raman line. This IR-inactive mode arises due to the lack of symmetry in the C–C bonds of the diamond crystal in the near surface region.

Fig. 2 shows the DRIFT results of the fluorination of the oxidized diamond powder surface [18]. Before fluorination, the spectrum shows a peak at 1788 cm^{-1} due to C=O stretching vibrations and several peaks at 1080, 1316, and 1470 cm^{-1} due to C–O stretching vibrations. After fluorination at or above 100 °C, the peak at 1788 cm^{-1} shifted to a significantly higher frequency. This indicates that C=O stretching vibrations are affected by fluorine atoms. The shifted peak can be composed of three bands. The most shifted peak is centered at 1884 cm^{-1}. In the case of carbonyl fluoride (COF), the peak of C=O stretching vibrations appears around 1890 cm^{-1}. This suggests that carbonyl fluoride groups were produced on the diamond surface. As contrasted with the fluorination of the hydrogenated diamond surface, most of the oxygen

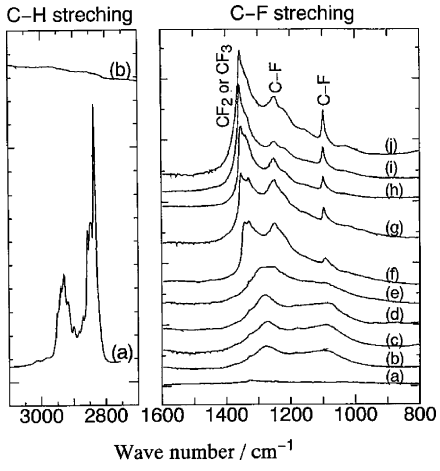

Fig. 1. DRIFT spectra of the hydrogenated diamond powder surface during fluorination: (a) before treatment, (b) treated in F_2 at −10 °C, (c) 0 °C, (d) 10 °C, (e) 35 °C, (f) 100 °C, (g) 200 °C, (h) 300 °C and (i) 500 °C.

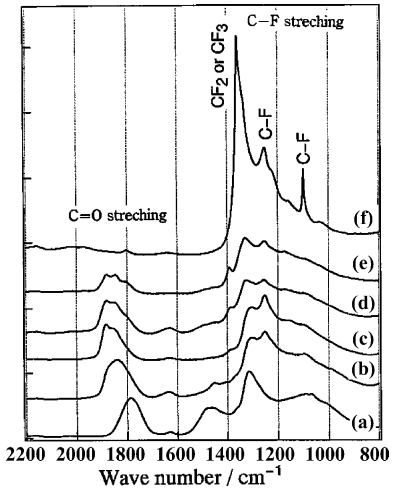

Fig. 2. DRIFT spectra of the oxidized diamond powder surface during fluorination: (a) before treatment, (b) treated in F_2 at 100 °C, (c) 200 °C, (d) 300 °C, (e) 400 °C and (f) 500 °C.

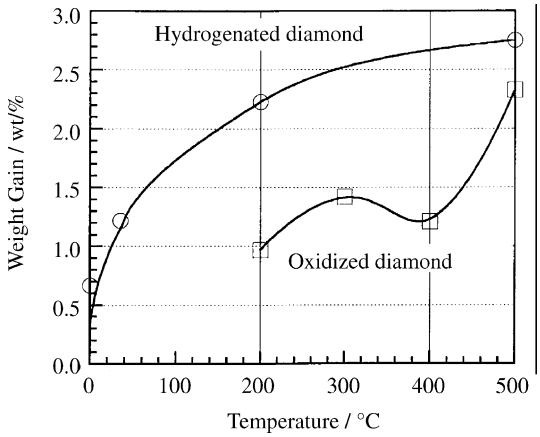

Fig. 3. Dependences of weight change of the diamond powders on the fluorination temperature for hydrogenated and oxidized diamonds. Curves are added to aid the viewer.

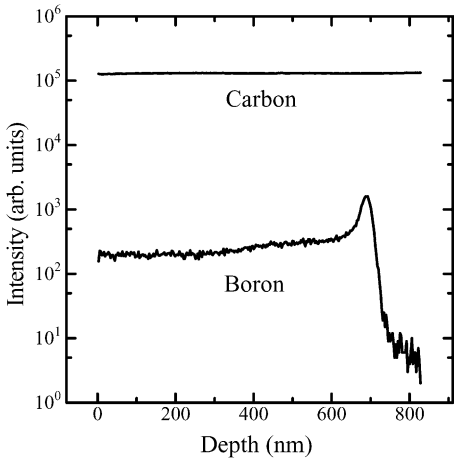

Fig. 4. SIMS depth profile obtained from the monolayer B-doped diamond thin-film sample. The boron to carbon ratio in the gas phase was 125 ppm.

chemisorbed on the diamond surface remains on the surface below 200 °C. The oxygen atoms bonded to the diamond surface with double bonds were affected by fluorination, but they could not be eliminated by fluorine molecules at low temperatures. Above 300 °C the peaks of C=O stretching vibrations decreased in intensity. At 500 °C a very small peak at 1800 cm^{-1} was observed and intense peaks of C–F stretching vibrations at 1099, 1252 and 1360 cm^{-1} appeared at 500 °C. These C–F stretching peaks are similar to those of the above-mentioned results on the hydrogenated diamond.

Fig. 3 shows the change in weight of the diamond powder after fluorination in F_2 at various temperatures [18]. The large specific surface area of ca. 20 $m^2\,g^{-1}$ allows the observation of the weight change due to surface reaction. No weight loss is observed in either of the samples indicating that diamond is chemically very stable and only the outermost surface of the diamond is fluorinated by 1 atm elemental fluorine at 500 °C. The curve for the hydrogenated diamond in Fig. 3 suggests that hydrogen atoms chemisorbed on the diamond surface have been substituted with fluorine atoms. The observed maximum weight gain of 2.7 wt.% corresponds to the chemisorption of two or three fluorine onto one carbon atom yielding CF_2 or CF_3 species. In the case of the oxidized diamond surface, the weight gain due to fluorination was smaller than that in the case of the hydrogenated diamond surface. As the desorption of C=O species and the adsorption of F occurs simultaneously below 400 °C, The curve for the oxidized diamond in Fig. 3 shows a relative maximum at 300 °C and then a decrease. The weight gain increased again above 400 °C because further adsorption of F progresses to form CF_2 and CF_3 species.

2.2. Secondary ion mass spectra of boron-doped diamond thin films prepared using BF_3

Fig. 4 and Fig. 5, respectively, show the depth profiles of C and B secondary ion observed for the monolayer and 4-layer BDD thin-film samples prepared using BF_3. In the 4-layer sample the first layer (layer 1 with B/C = 200 ppm in the gas phase) is in contact with the (1 0 0) surface of the diamond substrate. The depth profile was plotted assuming a linear relationship between depth and etching time. The SIMS total etching times, for the monolayer and 4-layer samples, respectively, were 1333 s and 1199 s, and the crater depths after SIMS measurements 690 and 600 nm. The SIMS etching rate is calculated to be ca. 0.5 nm/s and the diamond film growth rate ca. 70 nm/h. Fig. 2 indicates that the diamond growth rate did not grossly depend on the boron concentrations in the gas and the resultant solid phases.

In Fig. 4 the B profile shows an interface effect at the depth of ca. 690 nm, and the B concentration, in terms of the film formation process, gradually decreases and plateaus. The likely cause for the decrease and the plateau is the initial instability of the mass flow controller with a minimal BF_3 gas flow rate. The gradual stabilization of the whole apparatus affecting temperature and pressure during the synthesis might have also played the role. Similar features

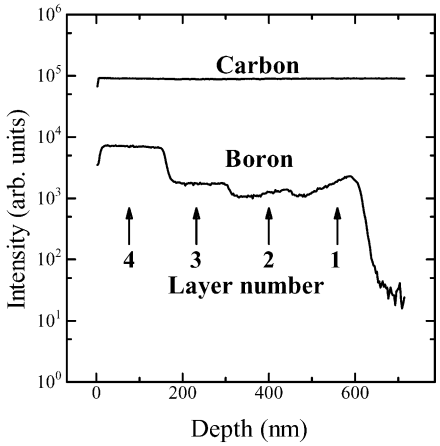

Fig. 5. SIMS depth profile obtained from the 4-layer B-doped diamond thin-film sample. The boron to carbon ratios in the gas phase were 250, 500, 1000 and 5000 for layers 1, 2, 3 and 4, respectively.

Table 1
BF_3/CH_4 in gas phase and boron concentrations in diamond film

BF_3/CH_4 in gas phase (ppm)	B concentration in diamond	
	cm^{-3}	B/C in ppm
125	6.3×10^{18}	36
200	5.0×10^{19}[a]	280[a]
500	5.0×10^{19}	280
1000	8.8×10^{19}	500
5000	3.3×10^{20}	1900

[a] The value is suspected to be larger than it ought to be (see text for explanation).

are observed in Fig. 5 for layers 1 and 2. As expected, the C concentration hardly changes. The relative sensitivity factor (RSF) of boron in diamond for O-SIMS has been reported to be 2.8×10^{21} cm^{-3} [27]. The concentrations of B atoms in the samples were calculated using the relationship $C_B = RSF_B \times I_B/I_C$ and are tabulated in Table 1, where C_B is the concentration of boron in diamond samples, and I_B/I_C is the ratio of the secondary ion counts of B and C. The B concentrations were calculated for the uppermost section of each layer. The B concentration found in the solid phase is plotted in Fig. 6 as a function of B/C in the gas phase, excluding the data point for layer 1 of the 4-layer thin-film sample owing to its clear unreliability as is seen from Fig. 5. A linear relationship is found for the B concentrations in the gas and solid phases [28,29], indicating that the boron atoms from BF_3 gas are indeed incorporated in the diamond matrix. The B-doping level and its dependence on gas phase B/C are found to be comparable to those found for (1 0 0) facet of B-doped CVD diamond using B_2H_6 [14,29], supporting the boron incorporation from BF_3.

2.3. Raman spectra of boron-doped diamond thin films prepared using BF_3

Fig. 7 shows Raman spectra of un-doped and B-doped diamond thin films prepared using BF_3 with various boron concentrations in the reactant gas phase [26]. The effect of

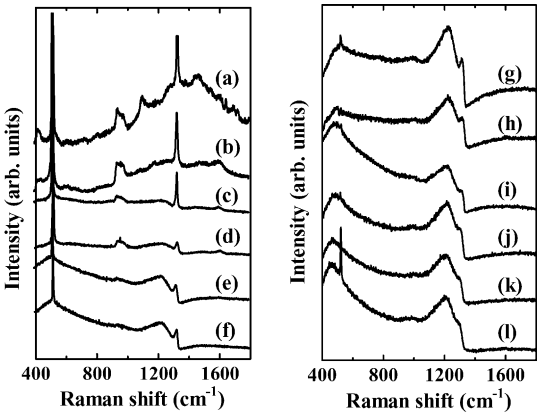

Fig. 7. Raman spectra of un-doped and B-doped diamond thin films with lower boron concentrations. B/C ratios in the gas phase are (a) 0 ppm, (b) 125 ppm, (c) 250 ppm, (d) 375 ppm, (e) 500 ppm, (f) 625 ppm, (g) 1000 ppm, (h) 1250 ppm, (i) 2000 ppm, (j) 2500 ppm, (k) 5000 ppm and (l) 10,000 ppm.

boron addition is clearly observed. In Fig. 7 the broad band centered at ca. 1500 cm^{-1}, assigned to disordered graphite is strong for the un-doped sample. It becomes barely observable for the sample with B/C = 125 ppm. At B/C = 125 and 250 ppm the one-phonon Raman peak at 1332 cm^{-1} becomes sharper. As the boron concentration further increases (B/C > 250 ppm), the graphite band becomes undetectable, and weak asymmetry and broadening appear in the one-phonon peak. At higher B/C ratios, the change in the profile of one-phonon band becomes progressively pronounced, and at the same time two broad bands around 500 and 1230 cm^{-1} appear. For the samples with much higher boron concentrations (B/C > 1000 ppm) the two broad bands at 500 and 1230 cm^{-1} become stronger and the asymmetry around the one-phonon peak becomes pronounced. These features are typical of BDD [14,30], indicating that BF_3 effectively acted as a boron source. Fig. 8 shows X-ray diffraction patterns of un-doped and B-doped thin-film samples [26]. The 1 1 1 and 2 2 0 reflections confirm that the bulk of the samples are indeed crystalline

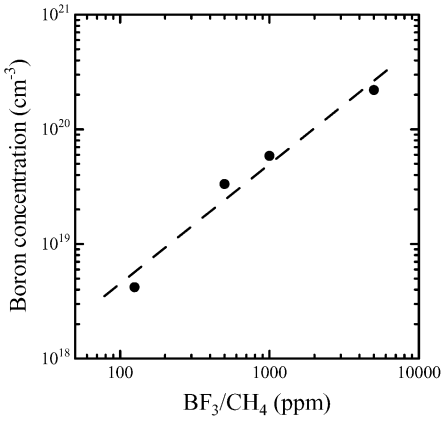

Fig. 6. Boron concentration found in the diamond matrix as a function BF_3/CH_4 in the gas phase.

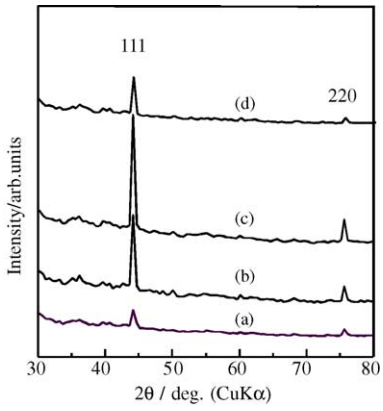

Fig. 8. X-ray diffraction patterns of un-doped and B-doped diamond films. B/C ratios in the gas phase are (a) 0 ppm, (b) 375 ppm, (c) 1250 ppm, (d) 5000 ppm.

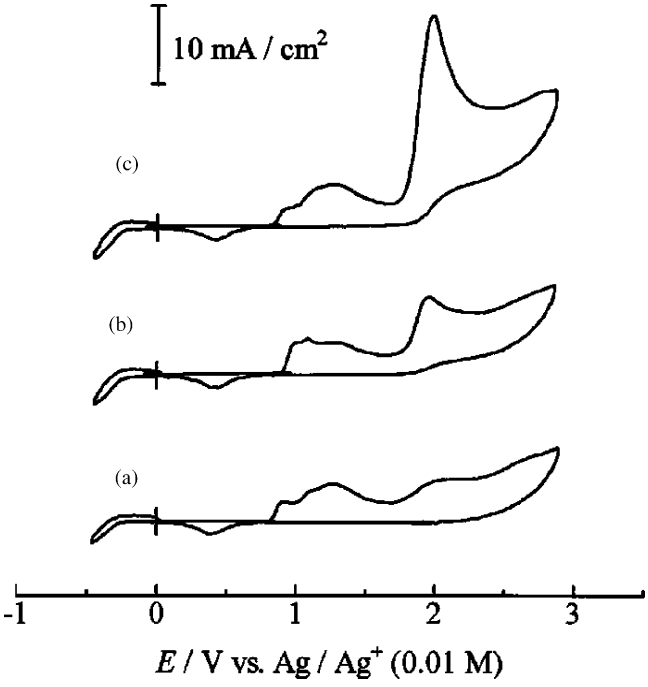

Fig. 9. Cyclic voltammograms for Pt electrode in $Et_4NF{\cdot}4HF$ of: (a) blank, (b) 0.01 M and (c) 0.03 M of 1,4-difluorobenzene.

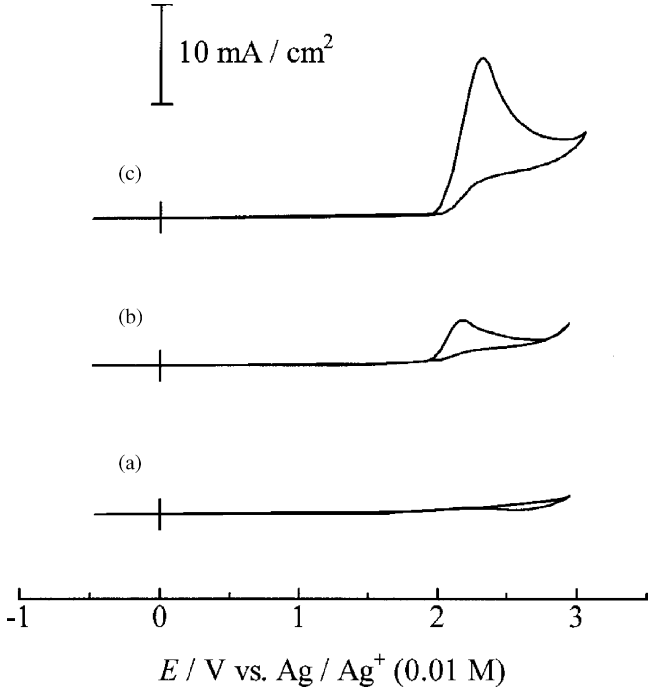

Fig. 11. Cyclic voltammograms for B-doped diamond electrode, prepared using B_2H_6, in $Et_4NF{\cdot}4HF$ of: (a) blank, (b) 0.01 M and (c) 0.03 M of 1,4-difluorobenzene.

diamond even for the sample with B/C = 5000 ppm, for which Raman one-phonon diamond peak is barely observed as a shoulder of the broad band around 1230 cm^{-1}.

2.4. Electrochemical behavior of semiconducting boron-doped diamond thin films prepared using B_2H_6 and BF_3

Fig. 9 and Fig. 10, respectively, show cyclic voltammograms (CVs) for Pt and HOPG in electrolyte solution

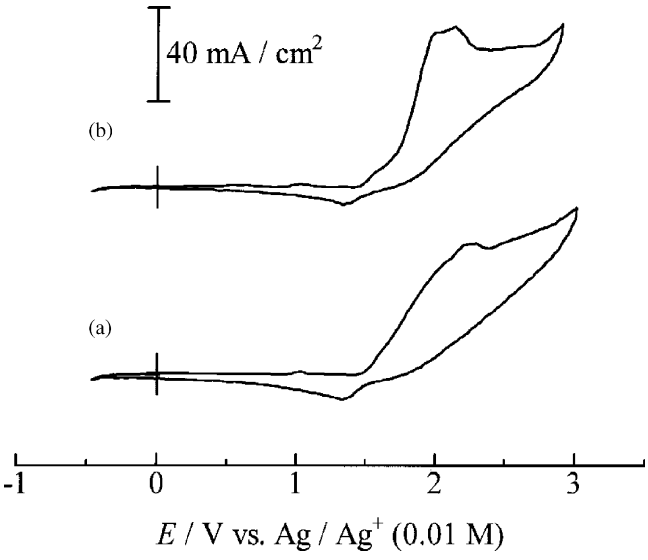

Fig. 10. Cyclic voltammograms for HOPG electrode in $Et_4NF{\cdot}4HF$ of: (a) blank and (b) 0.01 M of 1,4-difluorobenzene

$Et_4NF{\cdot}4HF$ to compare with those for BDD electrodes. Fig. 11 shows CVs for a BDD electrode prepared using B_2H_6. In the blank CV for the Pt electrode, Fig. 9(a), an oxidative wave is observed at 1–1.5 V (versus Ag/Ag^+) and a reductive wave at 0.4 V. The former is attributable to the formation of adsorbed oxygen or platinum oxide layer on the Pt electrode surface and the latter to the reduction of oxide layer [31]. This redox was probably caused by a trace amount of water in the electrolyte solution. The reduction peak below 0 V is assigned to the formation of hydrogen. In the blank CV for an HOPG electrode, Fig. 10(a), a pair of waves attributable to the intercalation (ca. 2.3 V) and de-intercalation (ca. 1.4 V) of fluoride ions are observed. Furthermore, in the blank CVs for Pt and HOPG electrodes, a broad rising peak towards higher potentials attributable to the oxidation of the electrolyte is observed. On the other hand, the blank CV for a diamond electrode, Fig. 11(a), shows essentially no waves in the same sweep range of −0.5–3.0 V (versus Ag/Ag^+) indicating its wide potential window. In this experiment the observation of rather large waves arising from a trace amount of water for Pt resulted in a clear manifestation of the wide potential window of diamond electrodes, since the same electrolyte was used for both Pt and diamond. These results indicate that diamond electrodes have higher current efficiency and stability than Pt and HOPG electrodes.

As 1,4-difluorobenzene is added, an oxidative wave appears at ca. 2.2 V in all cases as indicated by CVs (b) in Figs. 9–11. The peak height increases as the concentration of the added 1,4-difluorobenzene becomes higher from (b) to (c) in Fig. 9 and Fig. 11 for Pt and diamond electrodes,

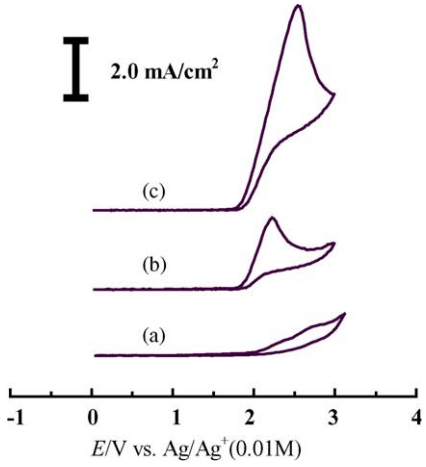

Fig. 12. Cyclic voltammograms for B-doped diamond electrode, prepared using BF_3, in $Et_4NF{\cdot}4HF$ of: (a) blank, (b) 0.012 M and (c) 0.025 M of 1,4-difluorobenzene.

respectively, indicating that this wave is attributable to the oxidation of 1,4-difluorobenzene leading to 3,3,6,6-tetrafluoro-1,4-cyclohexadiene [25,32]:

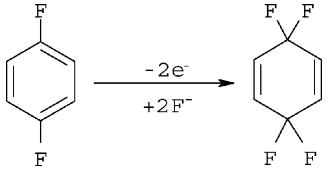

The results indicate that p-type semiconducting diamond has advantages of a wide potential window, high current efficiency and high chemical/electrochemical stability over Pt and HOPG electrodes for electrochemical fluorination. It is inferred that electrochemical fluorination in other systems and the electrolytic production of elemental fluorine would be possible at dimensionally stable diamond electrodes.

Fig. 12 shows CVs for a semiconducting diamond electrode prepared using BF_3. The blank CV shows a wide potential window of the diamond electrode, although a broad and small oxidative wave above 2 V is observed. In some of the cases where BDD prepared using BF_3 was used, no such anodic current was observed. The cause for the oxidative wave in this case is not clear. As 1,4-difluorobenzene is added, an oxidative wave appears at ca. 2.2 V. The peak height increases as the concentration of 1,4-difluorobenzene becomes higher from (b) to (c), indicating that this wave is attributable to the oxidation of 1,4-difluorobenzene. This electrochemical behavior is essentially the same as that of the BDD electrodes made using B_2H_6 explained above [25], confirming that BF_3 can be used as a boron source for the preparation of B-doped semiconducting diamond.

3. Conclusions

Diamond is chemically very stable, and only the outermost surface of diamond is fluorinated by 1 atm of elemental fluorine at 500 °C. BDD thin films were prepared using BF_3 for the first time by microwave plasma assisted CVD, and B concentration depth profiles were measured by SIMS. Raman spectra were taken to correlate the spectrum change with B-doping level. Electrochemical behavior of BDD electrodes prepared using BF_3 was studied by measuring CV for anodic oxidation of 1,4-difluorobenzene and compared with those made using B_2H_6. The chemical inertness of diamond and its wide potential window indicate that BDD can be used as an anode material for electrochemical fluorination and, possibly, for electrolytic production of fluorine.

4. Experimental

4.1. Fluorination of diamond surfaces and diffuse reflectance infrared Fourier-transform

Commercially available synthetic diamond powder less than 0.5 mm in diameter was used. The oxidized diamond surface was prepared by liquid phase treatment in a boiling acid mixture ($H_2SO_4 + HNO_3$) and the hydrogenated surface was prepared by vapor phase treatment in a pure hydrogen environment at 900 °C. Fluorination of the powders was carried out under fluorine pressure of 1 atm for 24 h at the treatment temperature. DRIFT spectra were recorded on a Bio-Rad Digilab FTS-45 FTIR instrument equipped with a liquid nitrogen cooled MCT detector in the region 4000–500 cm^{-1}. For each spectrum 256 scans were accumulated at a resolution of 2 cm^{-1}.

4.2. Preparation of boron-doped diamond thin films using BF_3, secondary ion mass spectroscopy, Raman spectroscopy and X-ray diffractometry

For SIMS measurements B-doped semiconducting diamond thin films were prepared by microwave plasma assisted chemical vapor deposition (CVD) on the (1 0 0) face of a 2 mm × 2 mm × 0.5 mm (Sumitomo Electric Industries, Ltd.) HP-HT single crystal diamond substrate using CH_4–H_2–BF_3–Ar. The process parameters used were as follows: 2.45 GHz, 450 W microwave source, 750 °C substrate temperature, 38 Torr total pressure, and 1% CH_4 in H_2. BF_3 was pre-diluted with Ar to 0.1%. Two samples were prepared: one with a fixed concentration of BF_3 in the feed gas (B/C = BF_3/CH_4 = 125 ppm) and the other one with four layers of BDD with increasing BF_3 concentration in the feed gas. The B/C gas concentration and reaction time are summarized in Table 2.

Depth profiles of B and C contents were determined by means of SIMS, CAMECA IMS-4f. A piece of gold mesh (#100, grid diameter = 70 μm) was attached to the surface of the samples to avoid charge-up because the samples were electrically insulating to semiconducting, and the samples were etched with O_2^+ ions [20,21,22]. Depth scales were

Table 2
B/C concentrations in the gas phase and reaction times for mono- and 4-layer B-doped diamond samples

Sample	Layer no.	B/C (ppm)	Reaction time (h)
Monolayer	–	125	10
4-Layer	1	200	2
	2	500	2
	3	1000	2
	4	5000	2

For the 4-layer sample the first layer (layer 1) is in contact with the (1 0 0) surface of the diamond substrate.

determined from measurements of the crater depths using a surface-profilometer (Veeco-Sloan, DEKTAK^{3}ST) after SIMS analyses. The spectra on F indicated that fluorine is unlikely to be incorporated in diamond matrix.

The samples for Raman spectroscopy measurements were prepared on the (1 0 0) face of silicon substrates. The B/C atomic ratio in the gas phase was varied in the range of 0–10,000 ppm. Raman spectra were recorded using a Renishaw Raman Microscope System 3000 using 632.8 nm line of a He–Ne laser with an output power of 25 mW.

X-ray diffraction patterns of diamond thin films were obtained on a Rigaku Rint 2200 using Cu Kα radiation.

4.3. Electrochemical behavior of semiconducting boron-doped diamond thin films prepared using B_2H_6 and BF_3

BDD thin-film using B_2H_6 was prepared by microwave plasma assisted chemical vapor deposition of a gas mixture of CH_4 and H_2 on a silicon substrate. The concentration of CH_4 in H_2 was 1%, and the ratio of B_2H_6 to H_2 was 10 ppm. The system pressure was kept at 38 Torr, and the flow rate of the gas mixture was 100 standard $cm^3\ min^{-1}$. The microwave power was 300 W and the reaction temperature of the substrate was 800 °C.

B-doped semiconducting diamond electrodes using BF_3 were prepared on the (1 0 0) face of silicon substrates as described in the previous section.

Electrochemical behavior of BDD thin-film electrodes was studied by measuring cyclic voltammograms (CVs) for anodic oxidation of 1,4-difluorobenzene in the liquid electrolyte, neat $Et_4NF{\cdot}4HF$ [25]. The electrolyte solution $Et_4NF{\cdot}4HF$ was prepared by adding anhydrous hydrogen fluoride to $Et_4NF{\cdot}2HF$ [33,34]. A diamond electrode was placed at the bottom of the cell with only the diamond thin film surface making contact with the electrolyte solution [35]. An $Ag/AgClO_4$ (0.01 M) in $Et_4N{\cdot}BF_4$ (0.1 M)/MeCN was used as the reference electrode [33,34]. The potential was scanned by means of a function generator (Hokuto Denko: HB-104) connected to a potentio/galvanostat (Hokuto Denko: HA-301). Blank background CVs were taken using Pt, HOPG and diamond electrodes before the addition of 1,4-difluorobenzene.

Acknowledgements

This work was supported in part by a Grant-in-Aid for 21st Century COE Program by the Ministry of Education, Culture, Sports, Science and Technology, and partly by Collaborative Research Project of Materials and Structures Laboratory, Tokyo Institute of Technology.

References

[1] N. Fujimori, T. Imai, A. Doi, Vacuum 36 (1986) 99.
[2] N. Fujimori, H. Nakahara, T. Imai, Jpn. J. Appl. Phys. 29 (1990) 824.
[3] D.M. Malta, J.A. von Windheim, B.A. Fox, Appl. Phys. Lett. 62 (1993) 2926.
[4] E. Yasu, N. Ohashi, T. Ando, J. Tanaka, M. Kamo, Y. Sato, H. Kiyota, Diamond Relat. Mater. 4 (1994) 59.
[5] M.C. Polo, J. Chifre, J. Esteve, Vacuum 45 (1994) 1013.
[6] S. Yamanaka, H. Watanabe, S. Masai, D. Takeuchi, H. Okushi, K. Kajimura, Jpn. J. Appl. Phys., Part 2 37 (1998) L1129.
[7] A.Ya. Sakharova, Yu.V. Pleskov, F.Di. Quarto, S. Piazza, C. Sunseri, I.G. Teremetskaya, V.P. Varnin, J. Electrochem. Soc. 142 (1995) 2704.
[8] N. Vinokur, B. Miller, Y. Avyigal, R. Kalish, J. Electrochem. Soc. 143 (1996) L238.
[9] H.B. Martin, A. Argoitia, U. Landau, A.B. Anderson, J.C. Angus, J. Electrochem. Soc. 143 (1996) L133.
[10] K. Okano, H. Naruki, Y. Akiba, T. Kurosu, M. Iida, Y. Hirose, T. Nakamura, Jpn. J. Appl. Phys. 28 (1989) 1066.
[11] T. Yano, D.A. Tryk, K. Hashimoto, A. Fujishima, J. Electrochem. Soc. 145 (1998) 1870.
[12] T. Yano, E. Popa, D.A. Tryk, K. Hashimoto, A. Fujishima, J. Electrochem. Soc. 146 (1999) 1081.
[13] L. Boonma, T. Yano, D.A. Tryk, K. Hashimoto, A. Fujishima, J. Electrochem. Soc. 144 (1997) L142.
[14] K. Ushizawa, K. Watanabe, T. Ando, I. Sakaguchi, M. Nishitani-Gamo, Y. Sato, H. Kanda, Diamond Relat. Mater. 7 (1998) 1719.
[15] D.E. Patterson, B.J. Bai, C.J. Chu, R.H. Hauge, J.L. Margrave, in: Proceedings of the 2nd International Conference on New Diamond Science and Technology, Material Research Society Symposium, MRS, Pittsburgh, PA, 1991, p. 433.
[16] D.E. Patterson, C.J. Chu, B.J. Bai, Z.L. Xiao, N.J. Komplin, R.H. Hauge, J.L. Margrave, Diamond Relat. Mater. 1 (1992) 768.
[17] M. Asmann, J. Heberlien, E. Pfender, Diamond Relat. Mater. 8 (1999) 1.
[18] T. Ando, K. Yamamoto, M. Kamo, Y. Sato, Y. Takamatsu, S. Kawasaki, F. Okino, H. Touhara, J. Chem. Soc., Faraday Trans. 91 (1995) 3209.
[19] N. Watanabe, T. Nakajima, H. Touhara, Graphite Fluorides, Elsevier, Amsterdam, 1988.
[20] Q. Chen, M.C. Granger, T.E. Lister, G.M. Swain, J. Electrochem. Soc. 144 (1997) 3806.
[21] G.M. Swain, R. Ramesham, Anal. Chem. 65 (1993) 345.
[22] H.B. Martin, A. Argoitia, U. Landau, A.B. Anderson, J.C. Angus, J. Electrochem. Soc. 143 (1996) L133.
[23] L. Boonma, T. Yano, D.A. Tryk, K. Hashimoto, A. Fujishima, J. Electrochem. Soc. 144 (1997) L142.
[24] T. Yano, D.A. Tryk, K. Hashimoto, A. Fujishima, J. Electrochem. Soc. 145 (1998) 1870.
[25] F. Okino, H. Shibata, S. Kawasaki, H. Touhara, K. Momota, M.N. Gamo, I. Sakaguchi, T. Ando, Electrochem. Solid-State Lett. 2 (1999) 382.
[26] F. Okino, Y. Kawaguchi, S. Kawasaki, H. Touhar, M. Nishitani-Gamo, T. Ando, in: G.M. Swain, T. Ando, J.C. Angus, W.D. Brown, J.L.

Davidson, A. Gicquel, W.P. Kang, B.V. Spitsyn (Eds.), Diamond Materials VII, 2001, pp. 103–107.
[27] S.P. Smith, M.I. Landstrass, R.G. Wilson, et al. in: A. Benninghoven (Ed.), in: Proceedings of the 8th International Conference on Secondary Ion Mass Spectrometry (SIMS VIII), 1992, pp. , p. 159.
[28] I. Sakaguchi, M. Nishitani-Gamo, K.P. Loh, K. Yamamoto, H. Haneda, T. Ando, Diamond Relat. Mater. 7 (1998) 1144.
[29] B.-J. Lee, B.-T. Ahn, Y.-J. Baik, Diamond Relat. Mater. 8 (1999) 251.
[30] P. Gonon, E. Gheeraert, A. Deneuville, F. Fontaine, L. Abello, G. Lucazeau, J. Appl. Phys. 78 (1995) 7059.
[31] A.J. Bard, L.R. Faulkner, Electrochemical Methods, Wiley, New York, 1980.
[32] K. Momota, M. Morita, Y. Matsuda, Electrochim. Acta 38 (1993) 1123–1130.
[33] K. Momota, M. Morita, Y. Matsuda, Electrochim. Acta 38 (1993) 619.
[34] K. Momota, T. Yonezawa, Y. Hayakawa, K. Kato, M. Morita, Y. Matsuda, J. Appl. Electrochem. 25 (1995) 651.
[35] F. Okino, H. Shibata, S. Kawasaki, H. Touhara, K. Momota, M. Nishitani-Gamo, I. Sakaguchi, T. Ando, in: Proceedings of the Tanso, No. 185, 1998, pp. , p. 306.